접착 및 계면 제25권 제4호, 2024년
〈연구논문(Original Article)〉

Journal of Adhesion and Interface Vol.25, No.4, 2024
https://doi.org/10.17702/jai.2024.25.4.128

Experimental Investigation of Carbon Fiber-reinforced Plastic Bonded with a DP6330NS Urethane Adhesive Using Single Lap-shear Joints under Fatigue Loading

Hyun-Bum Kim[1†] · Masafumi Niwano[2]

[1]*Mechanical Engineering, National Institute of Technology, Numazu College, 3600 Ooka, Numazu City, Shizuoka, 410-8501, Japan*
[2]*Advanced Materials Science & Engineering Course, National Institute of Technology, Numazu College, 3600 Ooka, Numazu City, Shizuoka, 410-8501, Japan*

(Received September 24, 2024; Revised October 09, 2024; Accepted October 21, 2024)

Abstract: Adhesive bulk specimens were fabricated to analyze the mechanical properties of DP6330NS. Non-contact video extensometer was used to measure the distances between two markers in the longitudinal and transverse directions during the tensile tests for the adhesive bulk specimens. Single lap-shear joints (SLJs) were fabricated to determine the fatigue life of carbon fiber-reinforced plastic bonded with a DP6330NS urethane adhesive. A digital microscope was employed to measure the area of voids on the fracture surfaces of the SLJs. The measured tensile strength and Young's modulus of the adhesive bulk specimens were 28.6 MPa and 2.05 GPa, respectively. Observation of the fracture surfaces on the SLJs revealed that the voids in the adhesive caused the fluctuation of the shear stress amplitude and shortened the fatigue life.

Keywords: *Fatigue, Adhesive, Carbon fiber-reinforced plastic, Single lap-shear joints, Voids*

1. Introduction

Joints bonded by adhesives are used in many industries, such as automotive, marine, and airplane [1-3]. Single lap-shear joints (SLJs) are employed to measure the strength in the overlap area because of their simplicity and applicability [4,5].

Aluminum alloys are widely used in automotive, aircraft, and construction industries [6-8]. Pereia et al. [9] studied the fatigue strength of an aluminum alloy AA 6082-T6 bonded with a high-strength epoxy adhesive. The SLJs specimens for treated with the etch with sodium dichromat-sulfuric acid on the aluminum alloy showed the maximum fatigue strength. Jen et al. [10] conducted fatigue tests using 5052-H32 aluminum alloy bonded with epoxy adhesive in SLJs. The results revealed that the fatigue strength increased as the adhesive thickness decreased. Sahin et al. [11] investigated the effects of adherend thickness (2～6 mm) on the fatigue strength using SLJs. AA2024-T3 aluminum alloys bonded with epoxy adhesive were subjected to fatigue tests. The results showed that applied maximum force increased as the adherend thickness increases in the fatigue tests. Gavgali et al. [12] investigated the fatigue life of AA2024-T3 aluminum alloy bonded with epoxy adhesive using SLJs. The SLJ specimens were compared with three-step-lap joints. The results revealed a decrease in the applied maximum force for the SLJ specimens compared with that of the three-step-lap joints specimens in tensile fatigue tests. Gamze et al. [13] prepared 7075-T7 aluminum alloy bonded with epoxy adhesive to investigate low-cycle fatigue using SLJs and used AISI 304 steel for comparison. The results revealed that the SLJs with steel showed a higher number of cycles than the aluminum specimens.

Adhesively bonded joints in composite materials have been used in various industries, e.g., aeronautics, automobile, and construction [14,15]. A study measured the static properties and fatigue life of carbon fiber/epoxy laminates bonded with a two-par epoxy adhesive using SLJs [16]. The results revealed that the specimens with a spew fillet at the end of the overlap length showed a 25% increase in

† Corresponding author: Hyun-Bum Kim (hyunbum.kim@numazu-ct.ac.jp)

fatigue strength compared with those with square edge joints. Carbon fiber-reinforced plastic (CFRP) plates bonded with an epoxy adhesive film using SLJs were subjected to three different surface treatments under static and fatigue loadings [17]. The specimens treated with sanding showed better fatigue endurance than the other specimens, i.e., grit blasting specimens and peel ply plus grit blasting specimens.

Urethane adhesives are used to join different materials for general use, structural, footwear, and food packaging industries [18-21]. An aluminum alloy 5754 bonded with a one-component polyurethane adhesive DINITROL 500 was studied under fatigue load using SLJs [22]. Fatigue tests showed that the SLJs with epoxy adhesives were more sensitive to fatigue load than those with polyurethane adhesive. Aluminum and glass adherends bonded with three different epoxy and one urethane adhesive were investigated using double-lap joints at high temperatures [23], and those with urethane adhesive showed larger displacement than those with epoxy adhesives. Double-lap specimens bonded with urethane adhesive showed a 27% increase in ultimate strength after one cycle of exposure to 85°C. Wei el al. [24] subjected aluminum alloy bonded with Sikaflex®-265 polyurethane adhesive to fatigue tests under different temperature conditions (−40∼80°C) using thick-adherend shear joints. The results showed that the fatigue performance of the thick-adherend shear joints decreased with the increasing temperatures. Lakshmana et al. [25] reported an improvement in fatigue life of polyurethane adhesive reinforced with microcrystalline cellulose and sawdust green fillers using SLJs. In the context of automotive applications, Kelly [26] measured the fatigue resistance of carbon fiber–epoxy laminates bonded with a two-component structural polyurethane adhesive (Pliogrip 7400/7410, Ashland Specialty Chemicals) using SLJs. Results revealed that the fatigue resistance of the hybrid (bonded/bolted) joints was greater than that of adhesive bonded joints. Moreover, material selection and joint design were found to be crucial for improving the fatigue resistance of the hybrid joints.

Most studies on epoxy and urethane adhesives measured the fatigue life using a limited number of specimens. The advantage of using a limited number of experimental data is to determine the trends of fatigue life in various parameters, e.g., adhesive thickness, adherend thickness, temperature dependency, and adhesive type. However, insufficient experimental data in fatigue tests can lead to errors in the reliability of structural adhesives.

This study was focused on the measurement of the shear stress amplitude of CFRP bonded with a DP6330NS urethane adhesive using SLJs. The area of voids in the SLJ fracture surfaces were investigated using a digital microscope to study the effects of voids on the fatigue life. The fatigue test results will provide material engineers with reliable information regarding CFRP/urethane adhesive joints. Tensile tests were also conducted on the adhesive bulk specimens to measure their mechanical properties, e.g., tensile strength and Young' modulus.

2. Experimental Methods

2.1. Adhesive bulk specimens

Silicone molds were punched out to produce dumbbell-shaped tensile test specimens. This shape was fabricated based on type 1 of JIS K 6251 [27]. A two-part urethane adhesive (3M^{TM} Scotch-weld^{TM} DP6330NS urethane adhesive) was poured into the silicone molds. The upper surface of the adhesive bulk specimens was polished with a #1500 sandpaper. The thickness and width of the adhesive bulk specimens were measured at three different locations using a micrometer (0.001 mm, Mitutoyo corporation, Japan). In total, six adhesive bulk specimens were prepared for tensile tests.

Tensile tests were conducted using a tensile testing machine (Autograph AG-X plus, Shimadzu Corp., Japan) at room temperature and a cross-head speed of 10 mm/min. The distances between two markers to the longitudinal and transverse directions during the tensile tests were recorded using a noncontact digital video extensometer (TRViewX, Shimadzu Corp., Japan), which was attached onto the front surface of the adhesive bulk specimen. Young's modulus and Poison's ratio were measured in the linear proportion regions between 0.1% and 0.5% in the stress (σ)–strain (ε) curves.

2.2. SLJs

A two-part urethane adhesive (3M^{TM} Scotch-weld^{TM} DP 6330NS urethane adhesive) and CFRP (plain weave board, thickness = 3 mm, TIP composite, Japan) were used as the adhesive and adherent, respectively. A thickness of 3 mm was selected for the adherent in accordance with the standard JIS K 6850 [28]. The CFRP surface was sandblasted for surface control. Ethanol was used to clean the CFRP surface after sandblast treatment. The adhesive was mixed manually for 1 min. Toggle clamps were used to hold and

press the adherents to produce SLJs. The average and standard deviation (SD) of the SLJ adhesive thickness were 0.04 and 0.02 mm, respectively.

2.3. Fatigue tests

Fatigue tests were conducted using servopulser servo dynamic systems (EHF-E Series, Shimadzu Corp., Japan). The waveform and speed of the fatigue tests were set as a sinusoidal waveform and 10 Hz, respectively. Fatigue tests were conducted under a constant load and in a room with an air conditioner set at 25°C.

Shear strength (τ_0) was measured using the following equation:

$$\tau_0 = \frac{P}{A_0}, \quad (1)$$

where P and A_0 represent the load and the total area of adhesives, respectively.

Shear stress amplitude (τ_{0_a}) was measured using the following equation:

$$\tau_{0\_a} = \frac{\tau_{0\_max} - \tau_{0\_min}}{2}, \quad (2)$$

where τ_{0_max} and τ_{0_min} represent the maximum and the minimum shear strengths, respectively. Stress ratio (R ratio = minimum shear strength/maximum shear strength) was set at -1. The fatigue limit for fatigue life was set at 10^7 cyclic loads.

3. Results and Discussion

3.1. Tensile tests for the adhesive bulk specimens

An image of an adhesive bulk specimen after a crack occurred is presented in Fig. 1. The crack was observed within the gauge length as shown in Fig. 1. The typical σ–ε curve of the adhesive bulk specimen is shown in Fig. 2, and the mechanical properties of the adhesive bulk specimens are summarized in Table 1. The average tensile strength and Yong's modulus were 28.6 MPa and 2.05 GPa, respectively.

3.2. Shear stress amplitude versus number of cycles to failure (S–N_f) plot

The typical load (P)–displacement (δ) curves of the SLJs is shown in Fig. 3; the datapoints represented by open circles, blue triangles, and red rectangles are obtained at 200,

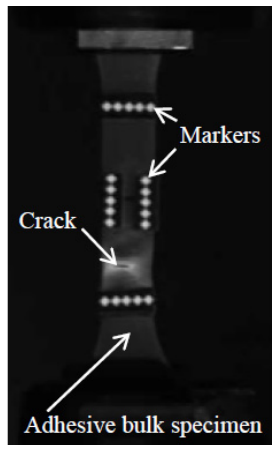

Figure 1. Image of an adhesive bulk specimen for the tensile test after a crack occurred.

Table 1. Mechanical properties of the adhesive bulk specimens

	Tensile strength σ [MPa]	Young's modulus E [GPa]	Poison's ratio ν	Fracture strain ε [%]
Average value	28.6	2.05	0.34	12.6
Standard deviation	1.31	0.19	0.10	13.2

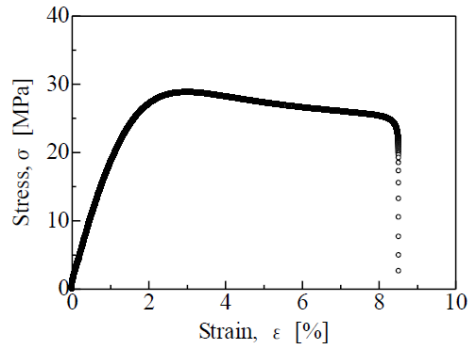

Figure 2. Typical stress–strain curve of the adhesive bulk specimens.

100000, and 900000 cycles, respectively. At constant maximum and minimum loads, the displacements increase with the increasing number of cycles.

The S–N_f plot derived using Eq. (2) is depicted in Fig. 4; the datapoints represented by open circles are obtained from the fracture specimens after the fatigue tests. The specimens with arrows represent the nonfracture specimens over 10^7 cyclic loads. Fluctuations in the shear stress amplitude are confirmed in Fig. 4.

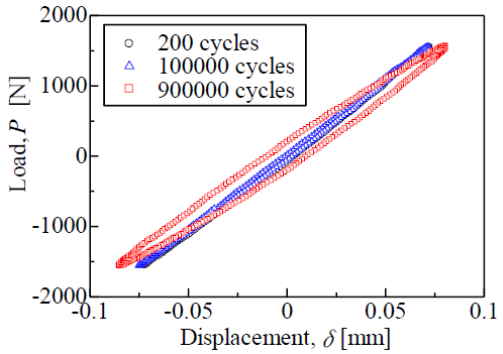

Figure 3. Typical load–displacement curves of the SLJs during fatigue tests conducted under a constant load.

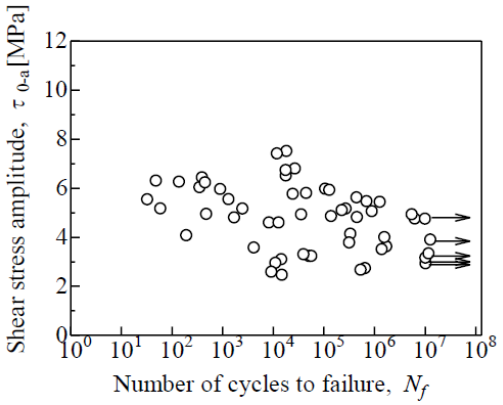

Figure 4. Shear stress amplitude versus number of cycles to failure for the SLJs.

3.3. Fracture surface observations

A digital microscope (VHX-8000, Keyence Corp., Japan) was used to observe the fracture morphology of the SLJs. A representative fracture surface of the SLJs is shown in Fig. 5. Fig. 5(B) is a magnified view of Fig. 5(A). Numerous round-shaped objects were observed on the SLJ fracture surfaces as displayed in Fig. 5(A). Fig. 6(A) illustrates a different type of SLJ fracture surface, and Fig. 6(B) presents a magnified view of Fig. 6(A). The beach marks indicated by arrows (a), (b), and (c) in Fig. 6(A) are attributed to fatigue behaviors. The white material marked by a black arrow is the fracture adhesive in Fig. 5(B) and 6(B).

Fig. 7(A) and 7(B) are the magnified views of the fracture adhesives in Fig. 5(A) and 6(A), respectively. Small-sized round particles marked by black arrows were observed on the SLJ fracture adhesives. This finding indicates that the adhesives were rubbed off owing to the shear behavior under fatigue load.

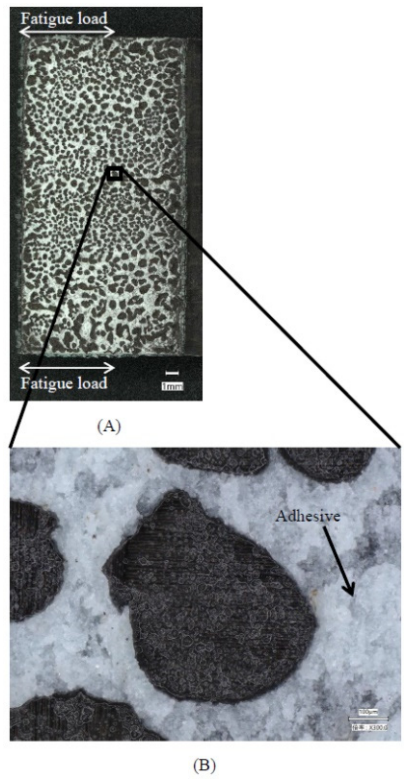

Figure 5. Fracture surface of the SLJs.

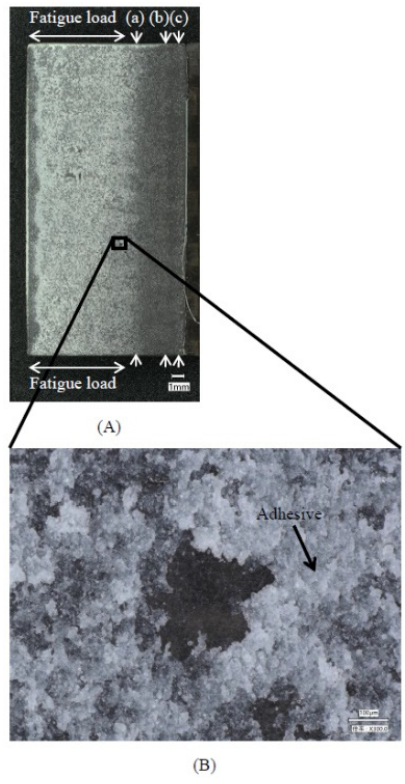

Figure 6. Fracture surface of the SLJs.

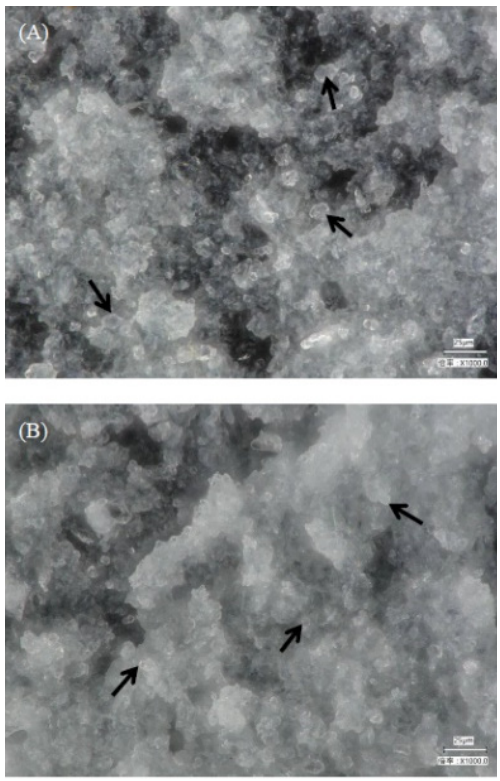

Figure 7. (A) and (B) are magnified views of the fracture surfaces shown in Fig. 5(A) and 6(A), respectively.

3.4. Void areas

Fig. 8(A) and 8(B) present the three-dimensional (3D) views of Fig. 5(B) and 6(B), respectively. Voids were observed on the SLJ fracture surfaces as marked by white arrows.

The areas of voids on the fractured surfaces were measured using a digital microscope to study the effect of the voids on the SLJs. As shown in Fig. 5(A) and 6(A), the measured areas of voids in the fracture surfaces were 45% and 11%, respectively. Normal distribution versus the area of voids is plotted in Fig. 9. The average void area and its SD in the fracture surfaces were 24.1% and 12.0%, respectively.

Shear strength (τ_1) was remeasured to consider the effect of the area of voids using the following equation:

$$\tau_1 = \frac{P}{A_0 - A_{voids}}, \quad (3)$$

where P represents the load. A_0 and A_{voids} represent the total area of adhesive including voids and the area of voids on the fractured adhesives, respectively.

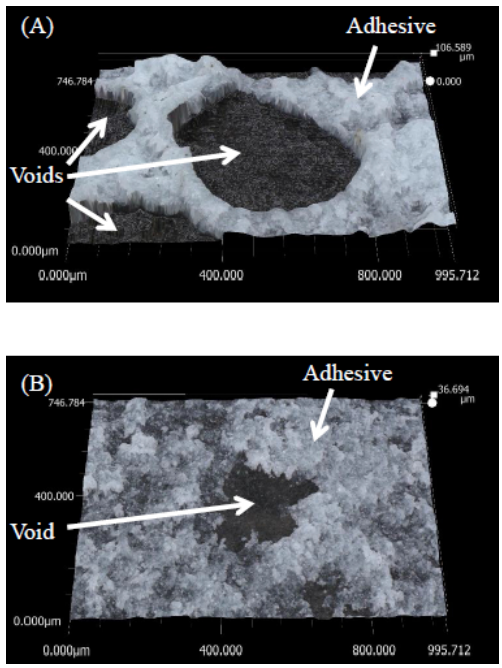

Figure 8. (A) and (B) are 3D views of the fracture surfaces in Fig. 5 (B) and 6 (B), respectively.

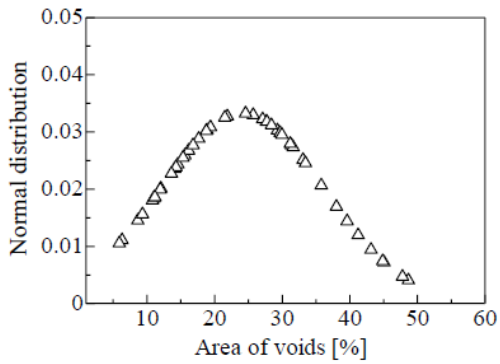

Figure 9. Normal distribution versus area of voids measured using a digital microscope.

Shear stress amplitude (τ_{1_a}) was also recalculated using the following equation:

$$\tau_{1\_a} = \frac{\tau_{1\_max} - \tau_{1\_min}}{2}, \quad (4)$$

where τ_{1_max} and τ_{1_min} represent the maximum and minimum shear strength considered the area of voids, respectively.

As mentioned in section 3.2, the SD was calculated using least squares method to evaluate the fluctuation of shear stress amplitude. SD was denoted as the residual standard

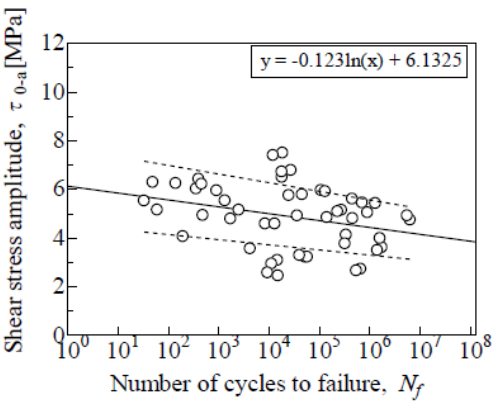

Figure 10. Shear stress amplitude versus number of cycles to failure. The data of the nonfractured specimen shown in Fig. 4 were excluded to evaluate the fluctuation. The two broken lines represent the SD.

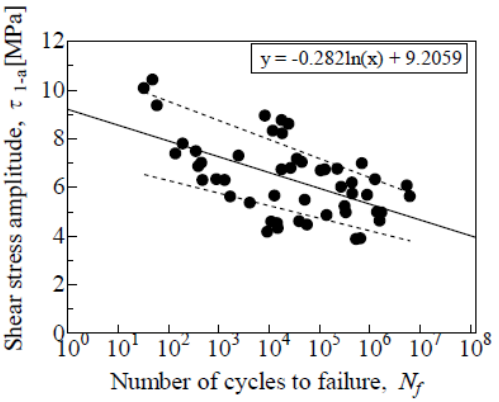

Figure 11. Shear stress amplitude versus number of cycles to failure. The data of shear stress amplitude were measured by considering the area of voids. The two broken lines represent the SD.

deviation (RSD), which was calculated using the following equation [29]:

$$RSD = \sqrt{\frac{\sum_{t=1}^{n}(x_i - f(N_f))^2}{n-1}}, \quad (5)$$

where, x_i and $f(N_f)$ are the i-th experimental data and a linear regression line. n represents the number of the experimental data.

The experimental data of S–N_f plot measured using Eq. (2) is depicted in Fig. 10, in which the nonfractured specimens were excluded. The black line represents a linear regression line. The two broken lines are the SD lines. The coefficient of variation (CV) measured using RSD for shear stress amplitude was 0.255.

The S–N_f plot measured using Eq. (4) is depicted in Fig. 11. The black line is a linear regression line. The two broken lines are the SD lines. The CV of shear stress amplitude measured using RSD was 0.206. Compared with the experimental value of 0.255, the calculated CV decreased by 19%. This finding means that if no voids are present in the adhesive of the SLJs, then the fluctuation of shear stress amplitude is expected to be low. A comparison of Fig. 10 and 11, reveals the shear stress amplitude are expected to be higher. A study was observed porosity on SLJ fracture surfaces using one-component polyurethane adhesive [30]. When the adhesive thickness was 0.3 mm in the SLJs, damage initially occurred at the substrate/adhesive interface and then the adhesive. SLJ fractured adhesives exhibited porosity, which resulted in a fatigue strength lower than those of other laser ablated joints [31]. However, these studies did not measure the actual areas of voids on SLJ fracture surfaces.

4. Conclusions

Fatigue tests were conducted to measure the fatigue life of CFRP bonded with a DP6330NS adhesive. Tensile tests were conducted on adhesive bulk specimens to measure their mechanical properties. Given the influence of voids on shear stress amplitude, the formed voids in the SLJ adhesive increased the fluctuation of the shear stress amplitude and decreased the fatigue life. Fabricating SLJs in a vacuum environment can be useful for reducing the number of voids in the aforementioned adhesive.

Acknowledgements

This research was funded by Sango Monodukuri Foundation Grant Number 2022-RD-01.

References

1. L. D. R. Grant, R. D. Adams, and L. F. M. da Silva, *Int. J. Adhes. Adhes.*, **29**, 405 (2009).
2. F. Dominguez, and L. Carral, *Brodogradnja*, **71**, 89 (2020).
3. M. G. Romano, M. Guida, F. Marulo, M. G. Auricchio, and S. Russo, *Mater.*, **13**, 1 (2020).
4. S. Shaikh, N. Anekar, P. Kanase, A. Patil, and S. Tarate, *Int. J. Curr. Eng. Technol.*, **7**, 2347 (2017).
5. F. Kadioglu, *Chin. J. Aeronaut.*, **34**, 154 (2021).

6. J. Hirsch, *Trans. Nonferrous Met. Soc. China*, **24**, 1995 (2014).
7. T. Dursun, and C. Soutis, *Mater. Des.*, **56**, 862 (2014).
8. E. Georgantzia, M. Gkantou, and G. S. Kamaris, *Eng. Struct.*, **227**, 1 (2021).
9. A. M. Pereira, J. M. Ferreira, F. V. Antunes, and P. J. Bartolo, *Int. J. Adhes. Adhes.*, **29**, 633 (2009).
10. Y. Jen, and C. Ko, *Int. J. Fatigue.*, **32**, 330 (2010).
11. R. Sahin, and S. Akpinar, *Int. J. Adhes. Adhes.*, **107**, 1 (2021).
12. E. Gavgali, R. Sahin, and S. Akpinar, *Int. J. Adhes. Adhes.*, **104**, 1 (2021).
13. G. İspirlioğlu-Kara, and A. Özel, *J. Sci. Rep.*, **55**, 146 (2023).
14. S. Budhe, M. D. Banea, S. de Barros, and L. F. M. da Silva, *Int. J. Adhes. Adhes.*, **72**, 30 (2017).
15. M. D. Banea, M. Rosioara, R. J. C. Carbas, and L. F. M. da Silva, *Compos. B. Eng.*, **151**, 71 (2018).
16. M. Quaresimin, and M. Ricotta, *Compos. Sci. Technol.*, **66**, 176 (2006).
17. S. Park, R. Roy, J. Kweon, and Y. Nam, *Compos. A Appl. Sci. Manuf.*, **134**, 1 (2020).
18. M. A. Perez-Liminana, F. Aran-Aıs, A. M. Torro-Palau, A. C. Orgiles-Barcelo, and J. M. Martın-Martınez, *Int. J. Adhes. Adhes.*, **25**, 507 (2005).
19. J. Vega-Baudrit, M. Sibaja-Ballestero, P. Vazquez, R. Torregrosa-Macia, and J. M. Martın-Martınez, *Int. J. Adhes. Adhes.*, **27**, 469 (2007).
20. José M. Arenas, Cristina Alía, Julián J. Narbón, Rosa Ocaña, and Cristina González, *Compos. B. Eng.*, **44**, 417 (2013).
21. Y. Qiao, J. Jiang, H. Li, X. Gui, J. Zhang, and Y. Zhang, *Adv. J. Food Sci. Technol.*, **12**, 705 (2016).
22. Y. Boutar, S. Naïmi, S. Mezlini, R. J.C. Carbas, L. F. M. da Silva, and M. B. S. Ali, *J. Adv. Join. Process.*, **3**, 1 (2021).
23. F. Marchione, and P. Munafo, *Constr. Build. Mater.*, **299**, 1 (2021).
24. W. Tan, J. Na, G. Wang, Q. Xu, H. Shen, and W. Mu, *Int. J. Adhes. Adhes.*, **107**, 1 (2021).
25. L. R. Bhagavathi, A. P. Deshpande, G. D. J. Ram, and S. K. Panigrahi, *Int. J. Adhes. Adhes.*, **105**, 1 (2021).
26. G. Kelly, *Compos. Struct.*, **72**, 119 (2006).
27. JIS K 6251, (2017).
28. JIS K 6850, (1999).
29. H. Kim, K. Goda, and K. Aoki, *Seikei-Kakou*, **27**, 347 (2015).
30. Y. Boutar, S. Naïmi, S. Mezlini, R. J. C. Carbas, L. F. M. da Silva, and M. B. S. Ali, *Int. J. Adhes. Adhes.*, **83**, 143 (2018).
31. F. Moroni, F. Musiari, and C. Favi, *Int. J. Adhes. Adhes.*, **97**, 1 (2020).